# Octahedral vs. trigonal-prismatic coordination and clustering in transition-metal dichalcogenides

**ARTICLE** *in* JOURNAL OF THE AMERICAN CHEMICAL SOCIETY · JUNE 1984

Impact Factor: 12.11 · DOI: 10.1021/ja00324a012

# Octahedral vs. Trigonal-Prismatic Coordination and Clustering in Transition-Metal Dichalcogenides

**Miklos Kertesz and Roald Hoffmann***

*Contribution from the Department of Chemistry and Materials Science Center, Cornell University, Ithaca, New York 14853.* *Received July 5, 1983*

**Abstract:** An electronic explanation, based on band calculations, is presented for the following trend in layered, transition-metal dichalcogenides—in $d^0$ complexes the metals prefer to enter octahedral holes in AB layers; then as the electron count increases, trigonal-prismatic holes in AA layers are favored; for $d^3$ one finds again octahedral structures, albeit distorted in such a way as to give chains of metal–metal-bonded diamonds. The symmetry-controlled interactions between chalcogen layers at various points in the Brillouin zone are behind the octahedral–trigonal-prismatic choice, and a Jahn–Teller distortion is responsible for the particular pattern of clustering in $ReSe_2$.

The transition-metal chalcogenides, $MX_2$, X = S, Se, display a characteristic layered structure. Two-dimensional slabs are formed by two layers of close-packed chalcogenide atoms sandwiching one metal layer between them. Then these $MX_2$ slabs are stacked, with just van der Waals contacts between the slabs.[1] A schematic representation is shown in **1**. The multitude of

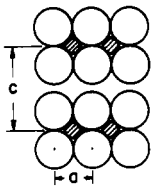


**1**

structural types that is found in these compounds is a consequence of the complex registry of chalcogenide and metal layers relative to each other.

There is one fundamental aspect of the structure that varies systematically through the transition series. The two chalcogenide layers forming a slab can be stacked directly above each other, making trigonal prismatic holes for the metals, **2**. Alternatively

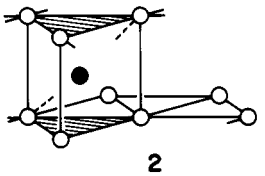

**2**

the layers may stagger, forming octahedral holes **3**. The 4B

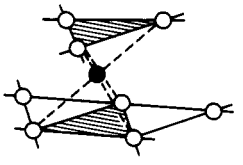

**3**

metals all have octahedral structures. For 5B metals most have octahedral structures while some have trigonal-prismatic geometries, and for 6B the reverse is true. In group 7B we find again octahedral structures, albeit distorted ones. Why this variation in preferred solid-state geometry?

The detailed nature of the deformations alluded to in group 7B dichalcogenides is intriguing. For instance, in the structure of $ReSe_2$,[2] **4** the Re atoms slip off from their regular octahedral

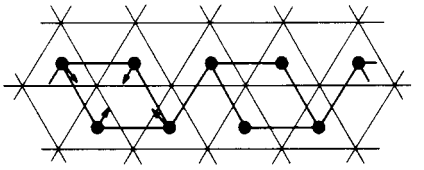

**4**

sites in such a way as to form approximate $Re_4$ units coupled to infinite one-dimensional chains. Is there an electronic reason for this deformation? That $ReSe_2$ is a semiconductor with a gap of $\sim$1.1 eV[3,4] is suggestive of this. The presence of charge density waves in most 5B dichalcogenides is also an indication of instabilities in the electronic structure of some of these systems,[4,5] instabilities tied to certain electron counts.

These regularities are the subject of this work. In what follows we first compare the band structures and total energies of the two different kinds of layers, trigonal-prismatic vs. octahedral, using a *rigid band model*; i.e., we shall use the very same band structure for different compounds across the Periodic Table. The study of such an *average band structure* is necessarily not accurate in its details, and for the individual compounds a number of band structures have been done which compare more favorably with experiment.[6] On the other hand, the rigid band model is, as we shall see, capable of accounting for the octahedral–trigonal-prismatic–octahedral trend as one moves across the transition series.

In the second part of the paper we shall derive the distorted $ReSe_2$ structure from the undistorted one. Throughout this work we shall employ simple tight-binding energy band structure calculations of the extended Hückel type,[7a] with some technical details listed in the Appendix.

(1) See: Hulliger, F. *Struct. Bonding (Berlin)* **1968**, *4*, 83. "Structural Chemistry of Layer-type Phases"; Levy, F., Ed.; D. Reidel: Boston, 1976; Vol. 5.

(2) Alcock, N. W.; Kjekshus, A. *Acta Chem. Scand.* **1965**, *19*, 79–84. The twinning in these has been described recently: Marolikas, C.; Amelinckx, S. *Physica B+C (Amsterdam)* **1980**, *99B*, 31–38.

(3) (a) $ReS_2$ and ReSeS are isostructural to $ReSe_2$: Wildervanck, J. C.; Jellinek, F. *J. Less-Common Met.* **1971**, *24*, 73–81. For another, more dense phase of $ReSe_2$, see: Larchev, V. I.; Popova, S. V. *Izv. Akad. Nauk SSSR, Neorg. Mater.* **1976**, *12*, 1365–67. (b) The isoelectronic systems $TcS_2$ and $TcSe_2$ have also distorted layer structures and a gap about 1 eV. See Wildervanck and Jellinek, ref 3a.

(4) Wilson, J. A.; Yoffe, A. D. *Adv. Phys.* **1969**, *18*, 193–335.

(5) (a) Peierls, R. "Quantum Theory of Solids"; Oxford University Press: London, 1955; p 108. (b) Friend, R. H.; Jerome, D. *J. Phys. C* **1979**, *12*, 1441–1477.

(6) (a) Matheiss, C. F. *Phys. Rev. B* **1973**, *B8*, 3719–3740. (b) Wexler, G.; Wooley, A. M. *J. Phys. C* **1976**, *9*, 1185–1200. (c) Doran, N. J. *Physica B+C (Amsterdam)* **1980**, *99B*, 227–237. (d) Ingelsfield, J. E. *J. Phys. C* **1980**, *13*, 17–36. (e) Myron, H. W. *Physica B+C (Amsterdam)* **1981**, *105B*, 120–122. (f) Friend, R. H. *Rev. Chim. Miner.* **1982**, *19*, 467–484. (g) MacDonald, A. H.; Geldart, D. J. W. *Phys. Rev. B* **1981**, *B24*, 469–472. (h) Bullett, D. W. *J. Phys. C* **1978**, *11*, 4501–4514.

(7) (a) See: Whangbo, M.-H.; Hoffmann, R. *J. Am. Chem. Soc.* **1978**, *100*, 6093–98. (b) Hoffmann, R. H.; Shaik, S.; Scott, J. C.; Whangbo, M.-H. Foshee, M. J. *J. Solid State Chem.* **1980**, *34*, 263–269.

0002-7863/84/1506-3453$01.50/0 

**Table I.** Selection of $c/a$ Ratios in $MX_2$ Transition-Metal Dichalcogenide Layers (X = S, Se)[a]

| trigonal-prismatic | | | octahedral | |
|---|---|---|---|---|
| compd | $c/a$ | | compd | $c/a$ |
| | | $d^0$ | | |
| | | | $TiS_2$ | 1.67 |
| | | | $ZrS_2$ | 1.59 |
| | | | $TiSe_2$ | 1.70 |
| | | $d^1$ | | |
| $NbS_2$ | 1.80 | | $TaS_2$ | 1.75 |
| $TaSe_2$ | 1.85[b] | | $VSe_2$ | 1.82 |
| | | $d^a$ | | |
| $MoS_2$ | 1.94 | | | |
| $WSe_2$ | 1.98 | | | |
| | | $d^3$ | | |
| | | | $ReSe_2$[c] | 1.92 |

[a] Only a few typical and extreme values are selected from more complete tables.[4] [b] Different polytypes have the following $c/a$: 2H (1.849), 3R (1.861), 4H (1.82). [c] Idealized.

### Trigonal-Prismatic vs. Octahedral Structures as a Function of the Electron Count

The d-electron count changes in going across the transition series. Since there are no bonding X–X contacts in these dichalcogenides (in contrast to trichalcogenides such as $NbSe_3$[7b]), we can safely assign formal oxidation state II to X, reaching oxidation state IV for the metals in $MX_2$. For example, Re in $ReSe_2$ will be taken as Re(IV), $d^3$.

In addition to the d-electron count variation across the series, packing considerations must enter. The trigonal-prismatic and octahedral holes are different size cavities for the metals, and the hole dimensions will depend on the size of the chalcogenide as well. A simple way to measure the cavity size is to compare the $c/a$ ratio. In the ideal close-packed trigonal-prism and octahedron arrangement (**5**) these are 2.0 and 1.633, respectively. Table I

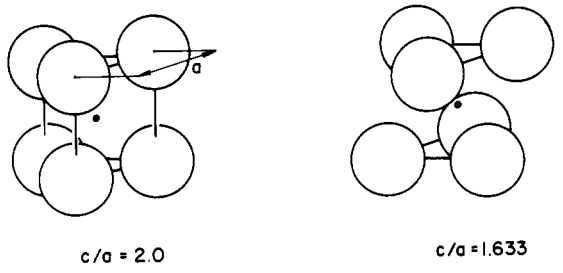


**5**

shows a selection of observed $c/a$ ratios in the chalcogenides. The deviations from the ideal ratios are a reflection of M–X and M–M bonding, among other factors. A strong argument for an electronic rationale for the choice between structural alternatives is to be seen in the observation that compounds choose between one and the other structure while having the same $c/a$ ratio. It must be said, however, that a good partitioning between octahedral and trigonal-prismatic structures was obtained by Gamble[8] based on ionic radii or on a plot of the radius ratios vs. fractional ionic character of the metal–chalcogen bond.

Packing considerations have dominated the solid-state literature for some time. Here we will concentrate on the electronic factors. In studying the above structural trend we shall focus on the differences between the energy band structure of the two different layers, the octahedral and trigonal prismatic. In order to bring out the effect of d-electron count most clearly, we shall take the band structure of an "average" compound, in our case alternative two-dimensional layers of $ReSe_2$ with an octahedral (undistorted)[9a] and a trigonal prismatic[9b] configuration. As it will turn out, the octahedral–trigonal-prismatic–octahedral trend is not very sensitive to the choice of metal, validating the use of the rigid band model.

Since we are interested in the difference between the octahedral and the trigonal-prismatic band structure, we shall first look at the band structures of the ligand systems only, free of the metal. We anticipate some differences due to the different packing, which is AB in the octahedral case and AA in the trigonal-prismatic case. Both layers are hexagonal, with the following Brillouin zone, **6**.

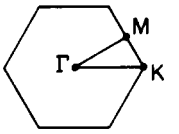


**6**

The irreducible wedge of the zone is enclosed by the lines connecting the special points Γ, M, and K. In what follows, k will denote a general point in the Brillouin zone; K will be reserved for the high-symmetry edge point. Although the total energy is the average of the occupied bands over the entire Brillouin zone,[10] discussion of orbitals at high symmetry points is of special concern to us, since these do determine the band structure to a considerable extent.

In discussing the main features of the band structure, we shall focus on the interplane interactions, because these give rise to the differences between the band structure of AA and AB. The unit cells of the two two-dimensional layers are shown in **7** and **8**.

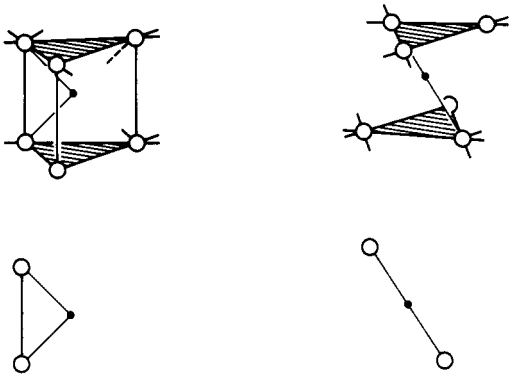

**7** **8**

The dark dot indicates the eventual position of the still absent metal and the lines the M–X axes. There is a 2-fold symmetry element in both cases, but it is a different one for the two structures—a mirror plane $\sigma_h$ for the AA double layer, an inversion center $i$ for the AB structure. Significant for the subsequent discussion is the fact that the nearest interlayer X–X contact is within one unit cell for AA, **7**, but between two different cells for AB, **8**.

Let us build up slowly the band structure of the two layers, taking Se as an example. Each Se enters with a 4s and three 4p levels. The choice of axes will be such that $p_z$ will be perpendicular to the layer ("out of plane") and $p_{x,y}$ in the layer ("in plane").

At the Γ point we expect two s (Se 4s) bands, symmetric and antisymmetric with respect to $\sigma_h$ or $i$. The splitting should be

(8) Gamble, F. R. *J. Solid State Chem.* **1974**, *9*, 358–367.

(9) (a) The geometry of the "undistorted" octahedral $ReSe_2$ layer is an idealization of the experimental[2] geometry with closed-packed Se and Re layers, with $a$ = 3.3 Å, and Re–Se distance of 2.49 Å, with Re atoms in octahedral holes. (b) The geometry of the trigonal-prismatic $ReSe_2$ layer model was taken to be most close to the octahedral one: all distances within the layers were kept fixed, as was the Re–Se distance.

(10) (a) Skriver, H. L. *Phys. Rev. Lett.* **1982**, *49*, 1768–1772. (b) See: Heine, V. "Group Theory in Quantum Mechanics"; Pergamon: London, 1960.

slightly larger for AA. At the same Γ point the in-plane $4p_x$ and $4p_y$ levels (four, altogether) will be pushed up because of in-plane interactions (see **9**, **10**). While the interaction of center 1 with

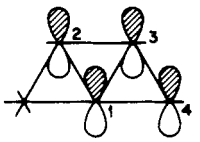


**9**

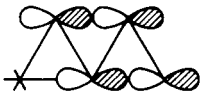

**10**

2 (numbering given in **9**) and 1 with 3 is antibonding, 1–4 is only weakly bonding. The other in-plane orbital, **10**, degenerate by symmetry with **9**, is 1–4 strongly antibonding, which dominates the character of this orbital. Then the **9–10** pair may be bonding or antibonding across the two layers, giving rise to a small splitting.

The $4p_z$ orbitals are not interacting strongly in plane, for X–X $\pi$ interactions, **11**, at a nonbonding separation between chalcogens,

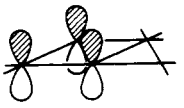

**11**

are weak. But the $4p_z$ orbitals will split into bonding and antibonding combinations due to interlayer or out-of-plane interactions. The two combinations are illustrated schematically in **12–14**.

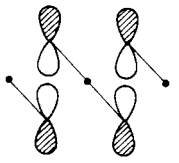

**12**

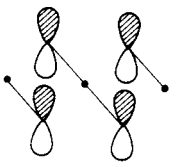

**13**

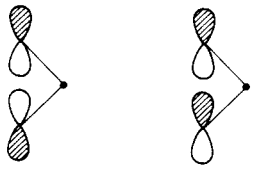

**14**

Note that the splitting is formally due to inter-unit-cell interactions in **12** and **13** but intracell interactions in **14**. Physically the interaction is similar—it is expected to result in a substantial splitting, and a greater one for the AA case where the overlaps are larger along the $z$ direction.

The case of the K point is quite different. Now, due to Bloch's theorem,[10b] a phase factor is associated to every translation. This factor is $e^{i\varphi}$, and $e^{-i\varphi}$ ($\varphi = 2\pi/3$) for one in-plane lattice vector translation, if they are chosen at 60° with respect to each other. As a consequence, certain degeneracies present in the AB (octahedral) system are lifted in the AA one. We will illustrate this for the AB octahedral hole case through the top view of the two combinations, **15** and **16**. The numbers on the atoms are proportional to the atomic orbital coefficients (appropriate for both $4p_z$ and 4s).

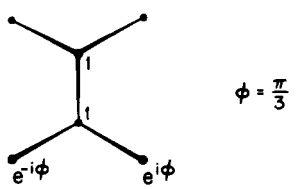


**15**

$\phi = \frac{\pi}{3}$

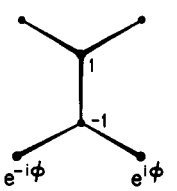


**16**

Orbitals **15** and **16** are degenerate, as are the famous $2p_z(\pi)$ orbitals of a single graphite layer at the K point in its Brillouin zone.[11] This can be seen most easily by examining the "bond order" or overlap population around the lower atom in these orbitals. The 1, 1 combination in **15** contributes a "bond order" of 1 to the overlap population, while the 1, $e^{i\varphi}$ and 1, $e^{-i\varphi}$ combinations are each antibonding, with "bond order" $-1/2$ each. The sum is 0. The sign of each contribution changes in **16**, but the total is still 0.[11]

In the AA packing the symmetry is lower; this degeneracy is split due to the interplane interactions. This splitting gives rise eventually to the energy gap in the trigonal prismatic case for $d^2$, causing the crossover of the stabilities of the octahedral and trigonal-prismatic structures between $d^2$ and $d^3$.

The in-plane $4p_x$ and $4p_y$ orbitals at K are slightly antibonding, and their splittings due to interlayer separations are small again.

Summarizing the general features of the two chalcogen layers' energy level scheme for these two high symmetry points, we obtain **17** for the octahedral and **18** for the trigonal-prismatic case.

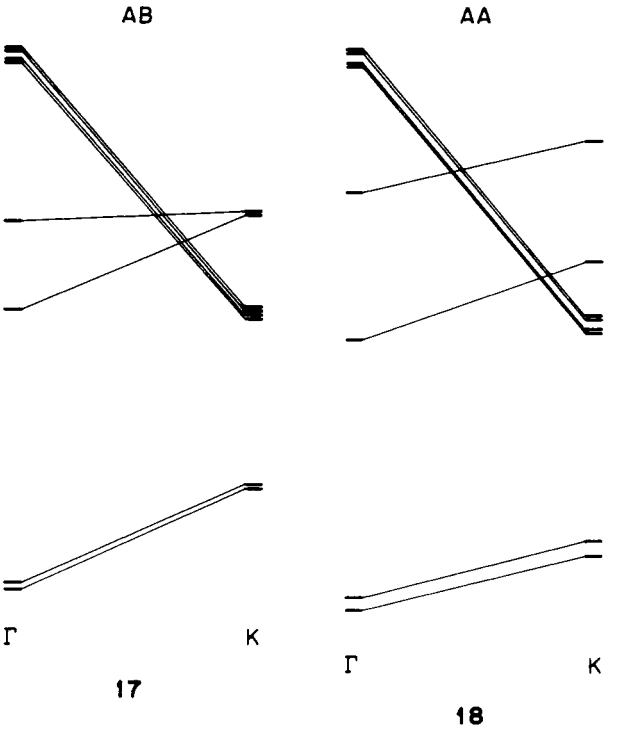


**17** **18**

The actual computed band structure is shown in Figure 1. Several necessary avoided crossings occur along the route from Γ to K, but the general trends are precisely those discussed above.

We proceed directly to the $MX_2$ structures by filling every octahedral hole of the AB layer with a transition metal M and every second trigonal-prismatic hole of the AA layer. The specific metal chosen is Re, and X is Se. The resulting band structures are shown in Figure 2.

Let us look first at the general features of these band structures. The p bands of either AA or AB layers of chalcogenides (Figure 1) lie between −10.5 and −16.5 eV. The resonance with Re 5d levels, placed at −12.66 eV, is excellent, as is the overlap between Re and its six neighbor Se atoms. Thus, there is substantial Re–Se interaction, splitting the Re d block. To put it into other words, the crystal field at Re is large. The expected consequence is a splitting of the Re d block into a three-below-two pattern. This is so for the octahedral case and also for the trigonal-prismatic

(11) A similar, well-known degeneracy occurs in graphite for the $\pi$-electrons at K. See: Wallace, P. R. *Phys. Rev.* **1947**, *71*, 622–634. Consequences of the symmetry of these graphite orbitals affecting C–C bond distances in graphite intercalation compounds have been discussed recently by us: Kertesz, M.; Vondervisztt, F.; Hoffmann, R. In "Intercalated Graphites"; Dresselhaus, M. S., Ed., Elsevier: Amsterdam, 1983.

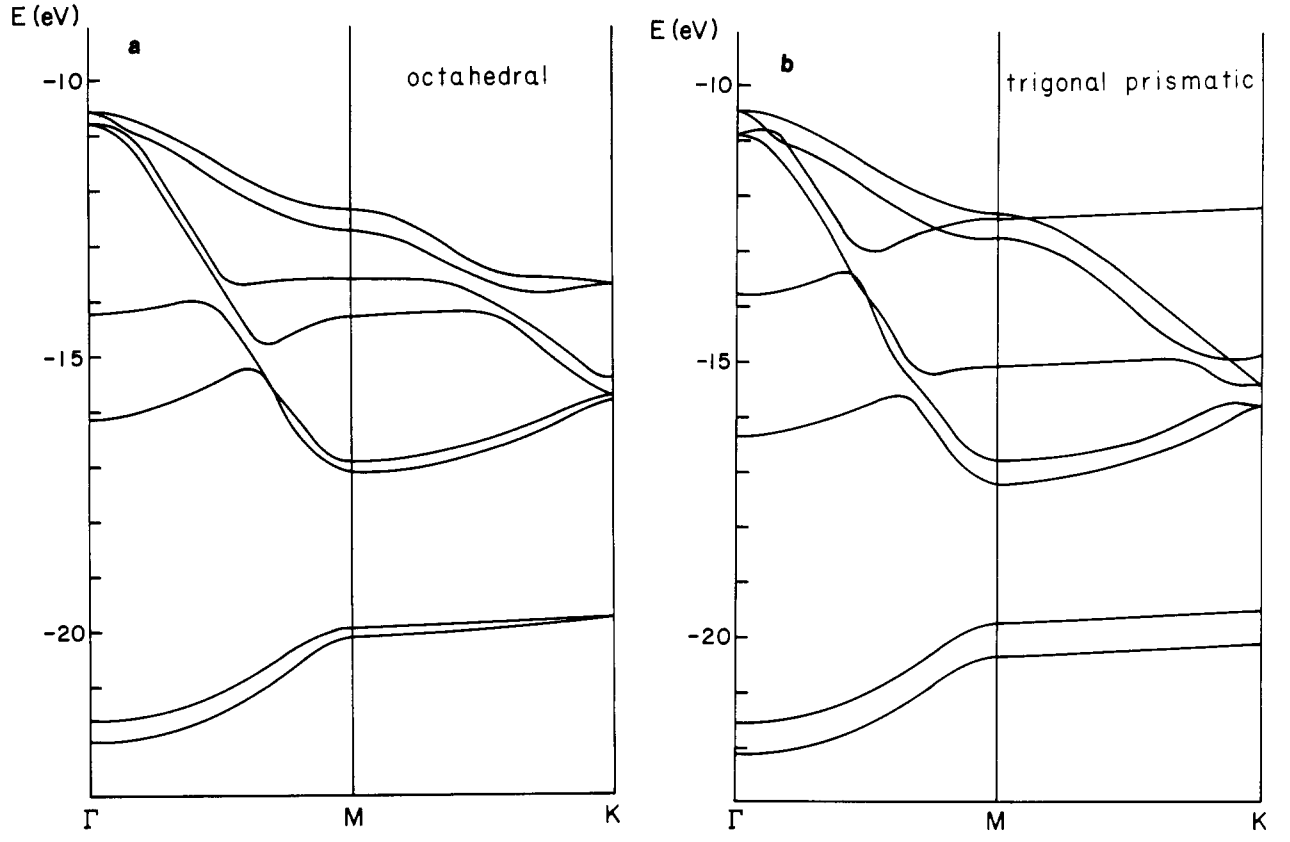


**Figure 1.** Energy band structure of two Se layers: (a) with octahedral (AB packing) and (b) with trigonal-prismatic holes (AA packing).

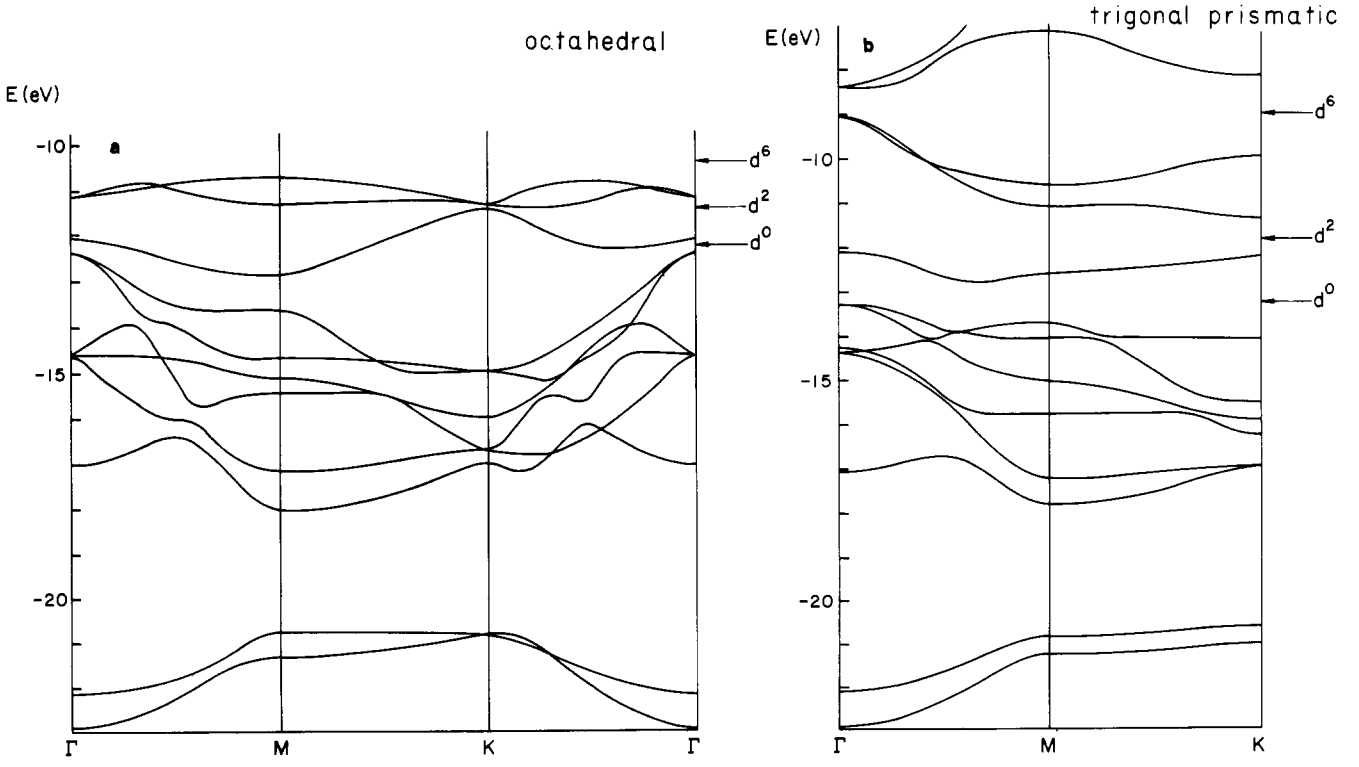


**Figure 2.** Energy band structures of $MX_2$ with Re and Se parameters: (a) octahedral[9a] and (b) trigonal-prismatic[9b] coordination around M.

one.[12] In the band structures of Figure 2 we see two Se s bands at low energy. Above these are six bands, largely Se p, and then three bands in the region between −9 and −13 eV which are largely Re d. These are the set of three alluded to above, and the Fermi level in the real dichalcogenide structures, electron counts $d^0$–$d^6$, will be in this region. The composition of the various bands is derived from projections of the density of states, shown in Figure 3.

(12) Hoffmann, R.; Howell, J. M.; Rossi, A. R. *J. Am. Chem. Soc.* **1976**, *98*, 2484–92. Huisman, R.; De Jonge, R.; Haas, C.; Jellinek, F. *J. Solid State Chem.* **1971**, *3*, 56–66.

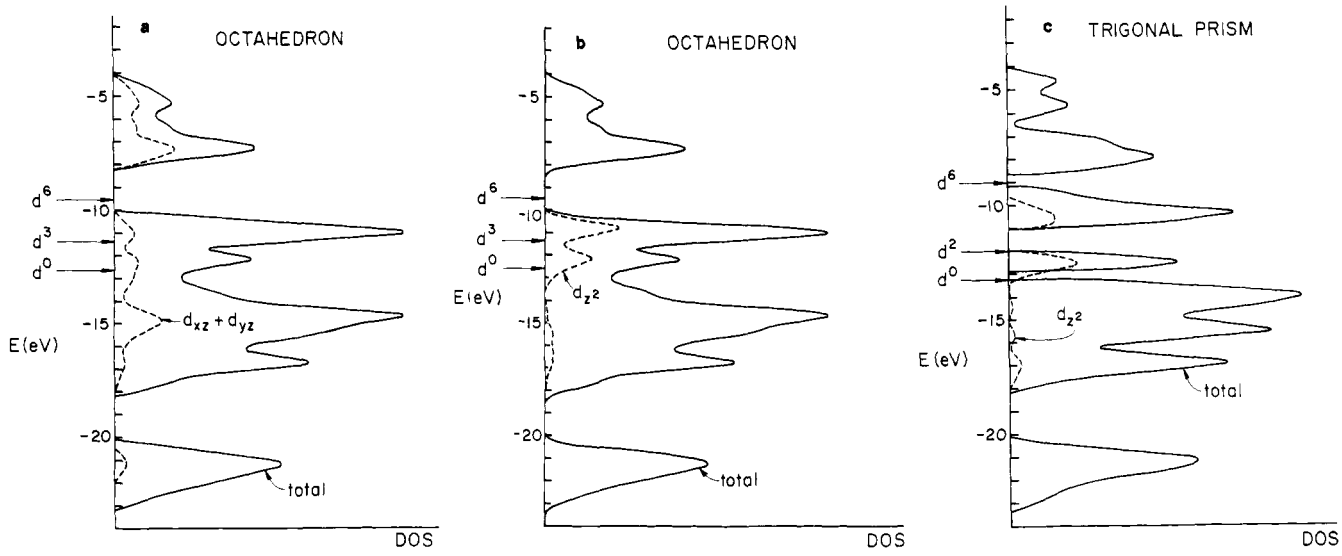


**Figure 3.** Density of states for an octahedral (a, b) and trigonal-prismatic (c) transition-metal dichalcogenide.[9] The dashed lines indicate projections into $d_{xz} + d_{yz}$ (a) and $d_{z^2}$ (b, c) orbitals, respectively.

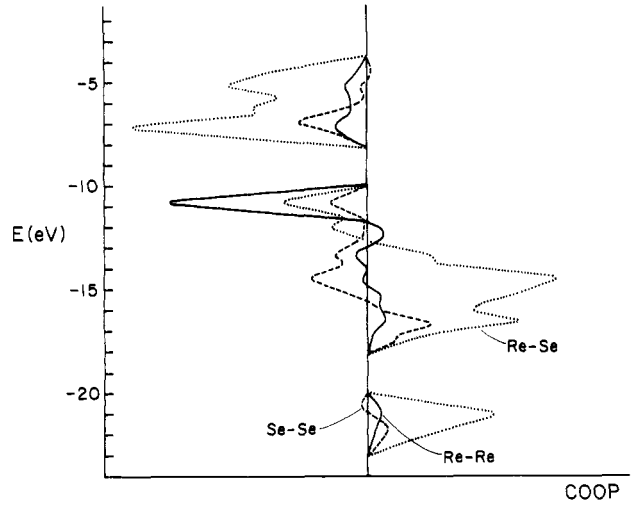


**Figure 4.** Crystal orbital overlap population (COOP) for Re–Re (—), Re–Se (- - -), and Se–Se (···) bonds in octahedral $ReSe_2$. The trend for the trigonal prismatic case is similar. Above −11 eV ($\sim d^3$ filling) all types of bonds become strongly antibonding and the layer structure becomes unstable.

The $d_{xz} + d_{yz}$ projection spreads out over a much broader energy range than the $d_{z^2}$ projection of the density of states, in accordance with the well-known ability of the $d_{xz}$ and $d_{yz}$ to interact more strongly with ligand orbitals than the $d_{z^2}$. However, the $d_{z^2}$ orbitals themselves do also spread out over a few eV. This is partly due to the metal–metal interactions. The peaks in the density of states between −9 and −13 eV have a strong $d_{z^2}$ contribution but also contain other orbitals. These characteristics are not fully in accord with the usual simplified picture based on crystal field arguments.[4]

The stability of the layered structure becomes small for electron counts over $d^3$, according to experience, and other (pyrites, marcasites) structures are observed for 8A group dichalcogenides, for instance.

Although we do not attempt to compare the $MX_2$ structures with those three-dimensional structures, it is worth looking at the crystal orbital overlap population curves displayed in Figure 4. (The trend for octahedral and trigonal prismatic is very similar.) Above −11 eV there is a negative peak for all these types of bonds (M–M, X–X, and M–X), indicating that filling much over this level destroys the structure, as such, although the M–X bonds could take up some more electrons. Also apparent is the dominating bonding character of the M–X bonds up to ∼−13 eV. The M–M bonds are weak and start to pick up some antibonding contribution in the middle of the d bands (at around −14 eV). The X–X bonds' first significant antibonding contribution from below is at ∼−15 eV, a rather low value, which is in the middle of the in-plane bands of the metal free ligands' bands (cf. Figure 1). Thus, the orbitals around the Fermi level for all $d^0$–$d^6$ electron counts are antibonding for X–X.

There are many interesting features of the band structure and density of states of these dichalcogenides, but let us focus in on the factor of prime interest to us, the difference between trigonal-prismatic and octahedral geometries.

For a $d^0$-electron count, bands 1 through 8 in Figure 2 filled, there is little difference in total energy between the trigonal-prismatic and octahedral layering, even though the details of the bands differ. Let us concentrate on bands 9 through 11, for it is these that will give a preference for one structure vs. another.

There are significant differences at Γ and K. At Γ bands 10 and 11 are shifted up in the trigonal prism relative to the octahedron. In the latter geometry the center of symmetry prevents one Se $p_{x,y}$ combination (**19**) from interacting with a d orbital,

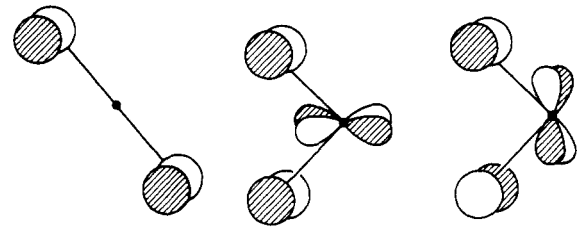

**19** **20a** **20b**

thus keeping its energy down. In the trigonal prismatic environment both $p_{x,y}$ combinations, **20a** and **20b**, can interact with d orbitals.

At K the differences can be traced to the same symmetry-lowering factor that in the metal-free bilayer produced a substantial splitting in the trigonal-prismatic arrangement. Band 9 goes down, band 11 up, relative to the octahedron. The energy gap at $d^2$ at the K point plays an important role in determining the stability of the two structures.[13] It is larger for the trigonal-prismatic case due to the same symmetry-lowering factor that in the metal-free bilayer produced a substantial splitting of the $4p_z$ orbitals in the trigonal-prismatic arrangement.

As we gradually fill these bands, first the trigonal-prismatic geometry will become relatively more stable, due to the downward shift of orbital 9 at K. This effect reaches its maximum around $d^2$, when an opposite trend starts, and the octahedral structure

(13) Py, M. A.; Haering, R. R. *Can. J. Phys.* **1983**, *61*, 76–84.

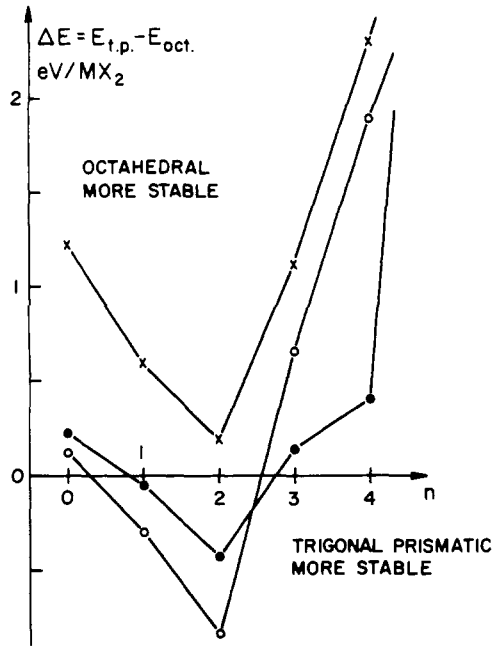


**Figure 5.** Relative stabilities of the octahedral and trigonal-prismatic coordination in an $MX_2$ layer, as calculated by the extended Hückel energy band theory. The three different series corresponds to three parameter sets: (●) $ReSe_2$ with the band structures of Figure 2; (○) $TiSe_2$ with Ti and Se parameters, but with $c/a = 1.94$; (×) $TiSe_2$ with experimental geometry. Connecting lines were provided to guide the eye.

will start to become more stable, due to the upward shift of bands 10 and 11 at Γ and M and band 11 at K. Figure 5 depicts the total energy differences as a function of the d-electron count. We repeated the calculation for $TiSe_2$ as well, a $d^1$ system, and a third time for $TiSe_2$ but with a different $c/a$ ratio.

The three curves reflect the same trend: for $d^0$ the octahedral structure is more stable; then filling the lowest d bands starts to favor the trigonal-prismatic structure. For still larger d-electron counts again the octahedral geometry is more stable. The crossover of the two effects is at $n = 2$. The whole trend is in agreement with the experimental findings summarized in the introduction. Most notable is the independence of this correlation of structure and d-electron count from the actual atomic parameters and the $c/a$ ratio. We have an electronic effect at hand, a consequence of the symmetry-controlled band structures at Γ and K. Experimental results of Py and Haering[13] on Li intercalation of $MoS_2$ indicate transformation of the layers from trigonal prismatic to octahedral. Assuming full charge transfer from Li to $MoS_2$ this is formally a $d^2$–$d^3$ transformation, which fits very well into the overall picture outlined above.

### The Clustering Distortion in $ReSe_2$

As mentioned earlier, the actual structure[2] of $ReSe_2$ can be viewed as a distorted ideal octahedral $MX_2$ layer compound. The distortion leads to formation of diamond-shaped $Re_4$ units chained together to form quasi-one-dimensional arrays, as illustrated in **21**. The unit cell of a two-dimensional layer-model is thus $Re_4Se_8$,

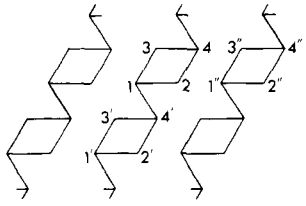

**21**

with 76 valence electrons filling 38 orbitals on average over the Brillouin zone. Our starting point will be the undistorted band structure, which will be first "backfolded", i.e., derived from the

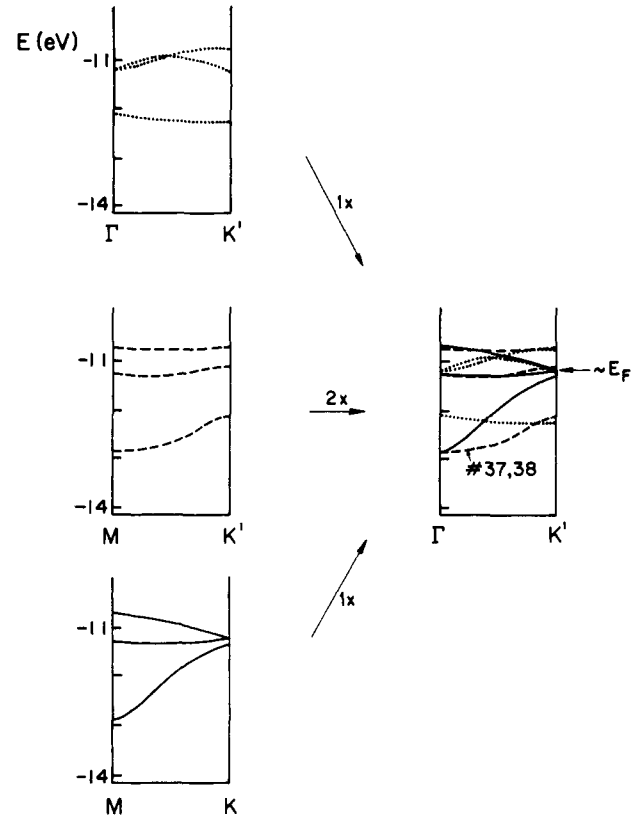


**Figure 6.** d bands along the Γ to K′ line in the back folded Brillouin zone for undistorted $Re_4Se_8$. (—) originates from M to K, (···) originates from Γ to K′, and (- - -) from M to K′ (twice). This band structure is derived from that of regular $ReSe_2$.

$ReSe_2$ band structure. The new unit cell ($Re_4Se_8$) is four times larger than that of the undistorted one; thus the new Brillouin zone is one-fourth of the original one, as illustrated on **22**. The

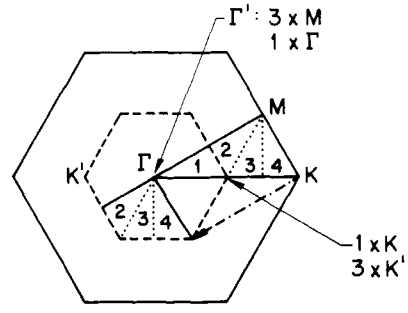


**22**

primed high-symmetry points refer to the new, small zone while those of the old, four times larger, are unprimed. Regions 1 through 4 are inequivalent in the old zone but are mapped to region 1 in the new one.

A number of new degeneracies occur at the new special points. These become important because after the distortion takes place some of the levels split strongly, in fact driving the distortion electronically. The new bands can be pieced together, slowly but systematically, from the previous band structure, using the mappings indicated in **22**. One such piecing-together process is illustrated in Figure 6.

In $Re_4Se_8$ 12 electrons have to be put into these bands ($d^3$). Of particular importance around the Fermi level are the triply degenerate bands (originating from M) and the doubly degenerate ones (originating from Γ), in the Γ′ point 37 through 41. Likewise, important are around the Fermi level the doubly degenerate levels (37 and 38) originating from K and the triply degenerate levels (39, 40, and 41) originating from K′, in the K′ point. These levels

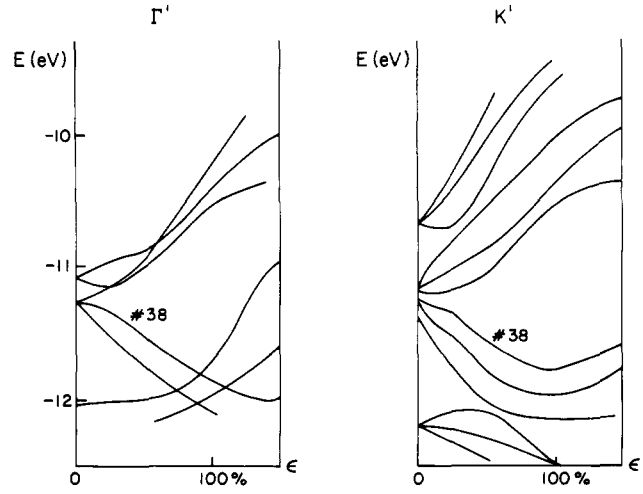


**Figure 7.** Walsh diagrams for the distortion of $ReSe_2$ for two points in the Brillouin zone. The distortion coordinate, $\epsilon$, is a parameter linearly connecting the undistorted ($\epsilon$ = 0) and the experimental ($\epsilon$ = 100%) geometry.

are derived from bands 9 through 11 of Figure 2a and have predominant $d_{x^2-y^2}$ and $d_{xy}$ characters. These d orbitals lie within a layer plane, and thus will be strongly affected by an in-plane distortion in which metal–metal overlaps are turned on. To put it another way, these in-plane bands will drive the distortion, if possible trying to open up a substantial band gap at the Fermi level.

Let us examine the detailed splitting of these bands as the distortion develops. In the Γ point band 39 is expected to be perturbed upward and 40 downward and 38 to remain at an intermediate energy. This is indicated schematically in **23**. If the downward perturbation is strong enough to shift 40 below 38, a distortion will be energetically favorable. Likewise, for the K′ point we expect a situation such as **24**. If the two levels (38, 39)

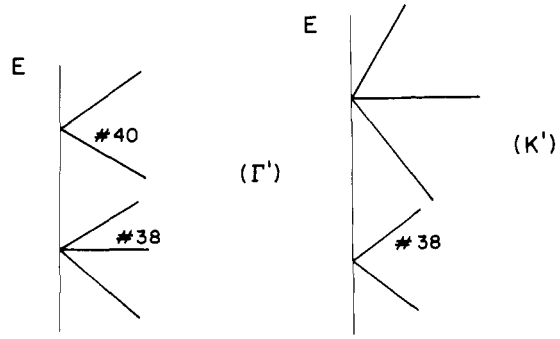


**23** **24**

are perturbed strongly enough, a distortion is preferred for that k-point. The actual situation, as represented by our band calculations, is shown in Figure 7. Here we have chosen a distortion parameter, $\epsilon$, which interpolates linearly between the undistorted octahedral $ReSe_2$ structure and the experimentally observed one.

Figure 7 is a Walsh diagram for two points, the most important ones, in the Brillouin zone. Similar things happen at both. Due to the lowered symmetry several avoided crossings occur. Especially the most important higher two orbitals (37 and 38) are pushed down by the presence of orbital 40, which is moved to lower energy by the geometrical perturbation at the Γ point and by orbital 39 at the K point. As a result, around $\epsilon$ = 25% distortion, the highest occupied levels move sharply to lower energy, driving the lattice to distort. How strong is this electronic distortion force? It is actually felt throughout the whole Brillouin zone, although to a varying degree. According to our calculations, the energy gain per $Re_4Se_8$ unit (at $\epsilon$ = 100%) is −2.54 eV at Γ′, −4.55 at K′, and −3.45 V on the average over the whole Brillouin zone. Due to the low symmetry and the large number of levels in close

**Table II.** $\Delta E = E(\epsilon = 0) - E(\epsilon = 100\%)$, for $Re_4Se_8$ in eV, as a Function of d-Electron Count

| $d^n$ | $d^0$ | $d^1$ | $d^2$ | $d^3$ | $d^4$ | $d^6$ |
|---|---|---|---|---|---|---|
| $\Delta E$ | −0.97 | 0.26 | 1.15 | 3.45 | 1.10 | −8.84 |

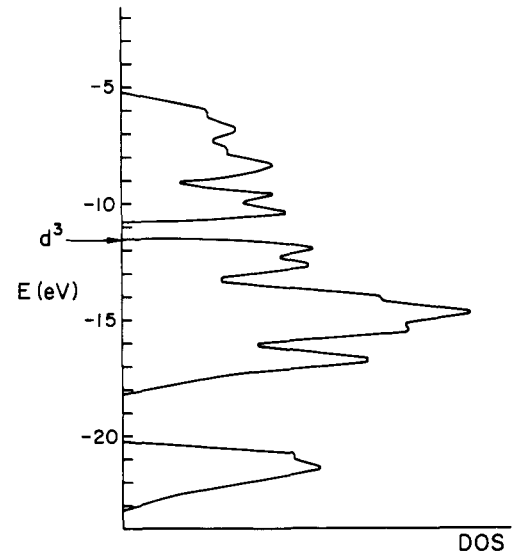


**Figure 8.** Density of states for the fully distorted model of $ReSe_2$.

proximity to each other, their character changes strongly along the distortion coordinate.

We can also look at the calculated total energy difference between the experimentally observed ($ReSe_2$) and the undistorted structure as a function of electron count. This is done in Table II.

The particularly large gain at the $d^3$ (Re) electron count coincides with the fact that the particular distortion observed in $ReSe_2$ is energetically favorable.

One consequence of this distortion is the opening of an energy gap in the band structure.[14a] This can be most readily seen in the density of states curve, as given in Figure 8. The gap is a consequence of the mutual repulsion of the orbitals around the Fermi level, as discussed in connection with the Walsh diagrams of Figure 7. The magnitude of our indirect, theoretical gap (0.87 eV) lies close to the experimental (optical) gap[3] of 1.15 eV for $ReSe_2$ and 1.33 eV for $ReS_2$, respectively. The calculated direct gap at Γ is 1.16 eV.

### Has $ReSe_2$ a Jahn–Teller- or a Peierls-Distorted Structure?

The above discussion of the distortion of $ReSe_2$ allowed us to trace back the driving force for the distortion to a Jahn–Teller type of splitting of orbitals. The splitting at small distortion values does *not* occur *at the Fermi level*, although close to it. But the level splitting is large enough to move the Fermi level, whose exact position is not essential for the actual distortion to occur.

This is in contrast to other, quite familiar, distortions widely occurring in quasi-one- and -two-dimensional systems as, e.g., polyacetylene,[14b] or several $d^1$ transition-metal dichalcogenides,[5] which are known under the names of Peierls distortion and periodic lattice distortions coupled to charge-density waves.[5b] For these instabilities, the periodicity of the distortion is related to particular dimensions and forms of the Fermi surface, which is often not commensurate with the periodicity of the lattice. These instabilities are most easily visualized in the language of energy band theory: the existence of large parallel "nesting" regions of the Fermi surface separated by a single wave vector $2\mathbf{k}_F$ leads to a strong

(14) (a) Application of the Mooser–Pearson rule (see: Hulliger, F.; Mooser, E. *Solid State Chem.* **1968**, *2*, 330) to the known structure would lead to the conclusion that the d electrons are localized in pairs, and that $ReSe_2$ is a nonmetal. See also: Torardi, C. C.; McCarley, R. E. *J. Solid State Chem.* **1981**, *37*, 393–397. (b) See: Kertesz, M. *Adv. Quantum Chem.* **1982**, *15*, 161–214.

(15) See: Schaad, L. J.; Hess, B. A.; Ewig, C. S. *J. Am. Chem. Soc.* **1979**, *101*, 2281–2283.

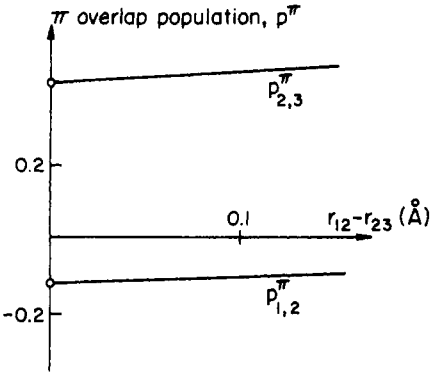


**Figure 9.** $\pi$-Overlap populations from a pair of quasidegenerate orbitals for cyclobutadiene as function of $r_{12} - r_{23}$ ($r_{12} + r_{23}$ = constant). The empty circles at $r_{12} - r_{23} = 0$ indicate that the values at this point are undetermined in Hückel theory.

scattering of the electrons with momentum $\pm\mathbf{k}_F$, splitting their energy strongly. Thus, an energy gap opens up and the system is stabilized. The periodicity of the potential, and thus that of the periodic lattice distortion, is tied in this picture to the particular $\mathbf{k}_F$. Without going further into this complex subject, it is already clear that the case of $ReSe_2$ is different in that neither the shape of the Fermi surface nor its energy is determining the particular "clustering" distortion of this semiconductor.

What then determines the particular deformation? Since three electrons occupy the three d-type bands, the distortion is such as to open a gap in the middle of it. Thus, the ratio of the number of bonding and antibonding regions should be roughly 1:1. For this to occur, doubling of the unit cell may be sufficient. However, for a system with the unit cell of $Re_2Se_4$, the number of short and long contacts cannot be 1:1 (in a lattice derived from a hexagonal one), in contrast to a one-dimensional system where this is easily fulfilled. On the other hand, for four units this condition may be fulfilled with the formation of the diamond shaped clusters of the experimental $ReSe_2$ structure.

In any molecular or extended system the overlap populations signal the way for a molecular distortion. By way of example let us step back from the crystal case to a molecular one, the simple Jahn–Teller system of cyclobutadiene, **25**. When $r_{12} = r_{23}$ the

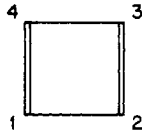


**25**

ground state is degenerate in Hückel theory. The overlap populations $p_{12}$ and $p_{23}$ from the degenerate orbitals are undetermined; they depend on the arbitrary choice of the occupied subspace within the degenerate two MO's. However, the slightest distortion toward $r_{12}-r_{23} \neq 0$ leads to definite $\pi$-overlap populations from these orbitals, $p^{\pi}_{12} < 0$ and $p^{\pi}_{23} > 0$, which do not depend strongly on $r_{12}-r_{23}$, as illustrated by an MO calculation for $C_4H_4$ in Figure 9.

In a similar way, it is informative to look at the overlap populations for the different metal–metal bonds in $ReSe_2$ at the very beginning of the distortion. For technical reasons, we have chosen a 1% deformation. Table III summarizes some of these overlap populations at different electron counts.

The $d^3$ count is particularly suitable for the formation of the chains as indicated in **21**: all bonds which will become shorter have larger overlap populations; those which will become larger are close to zero at $d^3$. The difference does not change dramatically even at 3% deformation, in analogy to the cyclobutadiene case. Thus, the wave function at very small deformation is already pointing into the direction of the actual deformation. The bond orders at the fully developed deformation are indicative of slight metal–metal bonding in the chains. We may conclude this section by answering the question posed in the subtitle: the distortion

**Table III.** $p_{IJ}$ Overlap Populations (× 1000) Averaged over the Whole BZ, as a Function of Electron Count, and Deformation for $Re_4Se_8$[a]

| | $\epsilon$ = 1% | | | | | $\epsilon$ = 3% | $\epsilon$ = 100% |
|---|---|---|---|---|---|---|---|
| | $d^0$ | $d^1$ | $d^2$ | $d^3$ | $d^4$ | $d^3$ | $d^3$ |
| intrachain | | | | | | | |
| 2,3 | 27 | 40 | 37 | 13 | −18 | 21 | 193 |
| 1,3 | 26 | 37 | 36 | 10 | −18 | 13 | 143 |
| 1,2 | 26 | 37 | 36 | 10 | −18 | 12 | 140 |
| 1,4′ | 26 | 36 | 36 | 10 | −19 | 11 | 89 |
| interchain | | | | | | | |
| 4,1″ | 26 | 33 | 33 | −0.4 | −22 | −1 | −32 |
| 2,1″ | 26 | 34 | 34 | 2 | −20 | 2 | −37 |

[a] Numbering according to **21**.

of $ReSe_2$ shows all the significant features of the molecular Jahn–Teller distortion.

A final remark about analogous systems: Recent X-ray and electron diffraction experiments[16] revealed the presence of a similar distortion in $MO_{2.065}S_3$, where the Mo atoms also slip off the octahedral interstices of a close-packed structure of sulfurs, forming diamonds, linked to chains like in $ReSe_2$. The formal d-electron count is very close to three here also.

The formation of molybdenum diamonds linked to chains is characteristic of the ternary compounds M□$Mo_2S_4$ (M = V, Cr, Fe, Co).[17] Their structure can be derived from the $MoS_2$ structure, but these are essentially 3-dimensional compounds, because the M transition metals coordinate to eight sulfur atoms, half of which belong to one $MoS_2$ layer and half to the next above it. To interpret spin susceptibility measurements[17c] on these systems, a model has been put forward,[17c] which assumes an oxidation state of II for M ($M^{2+}$). This would put the Mo's in a formal oxidation state $Mo^{3+}$, leading to $d^3$ formal count for the Mo's within the $MoS_2$ layers. Were it not for those interlayer bridgings we would be compelled to argue about a distortion of a regular Mo network toward the experimentally found one via a Jahn–Teller distortion of the type discussed in this paper.

**Acknowledgment.** We are grateful to Sunil Wijeyesekera for extensive and helpful discussions, to John Corbett for bringing the $MMo_2S$ work to our attention, to Jane Jorgensen for the drawings, and to Eleanor Stolz for the typing. Our research was generously supported by the National Science Foundation through Research Grant DMR 7681083 to the Materials Science Center at Cornell University. M.K. is on leave from the Hungarian Academy of Sciences.

## Appendix

The energy band structure calculations were performed by a program originally written by M.-H. Whangbo and extended by T. Hughbanks, S. Wijeyesekera, M. Kertesz, and Ch. Zheng in this group. The convergency with respect to the k point set has been checked, and most of the results reported refer to a 24 point set. It is proper to note that examination of only a couple of special points could be misleading, and therefore the orbital explanations given for the total energy changes are only justified a posteriori.

The atomic parameters used are as follows: Se:$H_{ii}(4s)$ = −20.5 eV, $H_{ii}(4p)$ = −14.4 eV; Slater exponents $\zeta(4s)$ = 2.44, $\zeta(4p)$ = 2.07. Ti:$H_{ii}(4s)$ = −8.97 eV, $H_{ii}(4p)$ = −5.44 eV, $H_{ii}(3d)$ = −10.81 eV; Slater exponents $\zeta(4s)$ = $\zeta(4s)$ = 1.5, $\zeta_1(3d)$ = 4.55, $\zeta_2(3d)$ = 1.44, with coefficients of 0.418 and 0.780, respectively. Re:$H_{ii}(6s)$ = −9.36 eV, $H_{ii}(6p)$ = −5.96 eV, $H_{ii}(5d)$ = −12.66; Slater exponents $\zeta(6s)$ = 2.4, $\zeta(6p)$ = 2.37, $\zeta_1(5d)$ = 5.34, $\zeta_2(5d)$ = 2.227, with coefficients of 0.638 and 0.566, respectively.

**Registry No.** $ReSe_2$, 12038-64-1; $TiSe_2$, 12067-45-7.

(16) Deblieck, R.; Wiegens, G. A.; Bronsema, K. D.; Van Dyck, D.; Van Tendelov, G.; Van Landuzt, J.; Amelinckx, S. In "Solid State Chemistry 1982, Proceedings of the 2nd European Conference"; Metselaar, R., Heijligers, H. J. M., Schoonman, R., Eds.; Elsevier: Amsterdam, 1983; pp 671–75.

(17) (a) van den Berg, J. M. *Inorg. Chim. Acta* **1968**, *2*, 216. (b) Guillevic, J.; Le Marouille, J.-Y.; Grandjean, D. *Acta Crystallogr., Sect. B* **1974**, *B30*, 111. (c) Chevrel, R.; Sergent, M.; Meury, J. L.; Quan, D. T.; Colin, Y. *J. Solid State Chem.* **1974**, *10*, 260.